

Influence of triangularity on the plasma response to resonant magnetic perturbations

S. Gu,^{1, a)} C. Paz-Soldan,² Y. Q. Liu,³ Y. Sun,⁴ B. C. Lyons,³ D. A. Ryan,⁵ D. Weisberg,³ N. Leuthold,² M. Willensdorfer,⁶ W. Suttrop,⁶ J.-K. Park,⁷ N. C. Logan,⁸ M. W. Shafer,⁹ H. H. Wang,⁴ Q. Ma,^{4, 10} A. Kirk,⁵ B. Tal,⁶ M. Griener,⁶ the ASDEX Upgrade,¹¹ and EUROfusion MST1 teams¹²

¹⁾*Oak Ridge Associated Universities, Oak Ridge, TN 37830, USA*

²⁾*Department of Applied Physics and Applied Mathematics, Columbia University, New York, NY 10027, USA*

³⁾*General Atomics, PO Box 85608, San Diego, CA 92186-5608, USA*

⁴⁾*Institute of Plasma Physics, CAS, P.O. Box 1126, Hefei 230031, China*

⁵⁾*CCFE, Culham Science Centre, Abingdon, OX14 3DB, UK*

⁶⁾*Max Planck Institute for Plasma Physics, 85748 Garching, Germany*

⁷⁾*Princeton Plasma Physics Laboratory, Princeton, New Jersey 08543, USA*

⁸⁾*Lawrence Livermore National Laboratory, Livermore, CA 94550, USA*

⁹⁾*Oak Ridge National Laboratory, PO Box 2008, Oak Ridge, Tennessee 37831, USA*

¹⁰⁾*University of Science and Technology of China, Hefei 230026, China*

¹¹⁾*See the author list of H. Meyer et al. Nucl. Fusion 59 112014 (2019)*

¹²⁾*See author list at Labit B. Et al., Nucl. Fusion 59 086020 (2019)*

(Dated: 28 February 2022)

The effect of the axisymmetric plasma shape to the non-axisymmetric plasma response to resonant magnetic perturbations (RMPs) is investigated in experiment and modeling for the DIII-D, EAST and ASDEX Upgrade tokamaks. Systematically modeling the effect of the triangularity, whilst keeping other equilibrium quantities largely unchanged reveals that the plasma response is strongly suppressed at high triangularity compared to that at low triangularity. This is validated through targeted comparison with experiments at DIII-D, EAST, and ASDEX Upgrade. DIII-D and EAST magnetic measurements are used to validate simulations, while at ASDEX Upgrade the plasma edge displacement is measured. Both experiments and modeling find a reduced magnetic plasma response on the high-field side at high triangularity across devices. Multi-modal analysis of the simulation results extracts the mode structure and applied spectrum dependence of each mode. The amplitude of the dominant mode reveals similar trends with the edge resonance and radial displacement near X-point, which suggests that the multi-mode plasma response provides another way to understand the edge localized mode (ELM) control physics. The plasma response is strongly reduced at high triangularity compared to that at low triangularity, which implies different ELM control effects as shaping is varied. These findings indicate that the plasma shape should be taken into consideration when designing an RMP-ELM control strategy in experiment, and that predictive plasma response calculations can be used to maximize access to RMP-ELM control in future devices by maximizing the coupling between coils and the plasma.

PACS numbers: 52.30.Cv, 52.35.Py, 52.55.Fa, 52.55.Tn

Keywords: plasma response, triangularity, RMP, ELM control

^{a)}Electronic mail: gus@fusion.gat.com

I. INTRODUCTION

The resonant magnetic perturbations (RMPs) produced by magnetic coils outside the plasma have been demonstrated¹ to be an efficient technique to control edge localized modes (ELMs), which can cause plasma facing components to erode at an unacceptable level for next generation fusion devices like ITER². This technique has been experimentally proven to be an effective method for either mitigating or suppressing ELMs on several tokamaks, including DIII-D³, JET⁴, MAST⁵, ASDEX Upgrade⁶, KSTAR⁷, EAST⁸, and HL-2A⁹.

Despite the fact that the physics of RMP-ELM control is not fully understood yet, the plasma response to RMPs is known to play significant role in this process^{10–12}. Many factors can affect plasma response and ELM control effect, and these have been intensively studied in the past few years. For instance, the shielding or amplifying effects caused by plasma profiles, such as the rotation^{13,14} or pressure^{15,16}, can result in a reduction or enhancement of the plasma response and in turn affect the plasma stability; the non-linear effects in plasma response are observed and found to be non-negligible in achieving ELM suppression^{8,17–19}; the multi-mode effect is found to be one essential feature of plasma response and can be used to optimize ELM control^{20–24}.

One particularly interesting aspect in controlling ELMs with RMP is the effect of the axisymmetric plasma shaping, such as the up-down asymmetry^{25,26} and triangularity of the plasma shape^{27–29}. In this work, the influence of triangularity on plasma response to RMPs is discussed. Statistical analysis of recent RMP-ELM control experiments in DIII-D found significant differences in the window of ELM suppression with different plasma triangularities²⁷, as shown in Figure 1(a), that ELMs are easier to suppress at upper triangularity $\Delta_{up} \sim 0.3$ compared to $\Delta_{up} \sim 0.1$, while suppression was not observed at $\Delta_{up} \sim 0.6$. Similar effects are also observed in ASDEX Upgrade²⁸ where ELMs are easier to suppress at upper triangularity $\Delta_{up} \sim 0.25$, as shown in Figure 1(b).

To understand the differences of ELM control effects with different triangularity, two possible hypotheses are proposed. One is that the plasma response to RMPs changes with triangularity, which affects the ELM suppression threshold and window. The other is that the 3D peeling-ballooning stability changes with triangularity, which in turn affects the ELM behavior. In this paper, we focus on the first hypothesis, and systematically investigate the influence of plasma triangularity on the plasma response to RMPs and the coupling to the

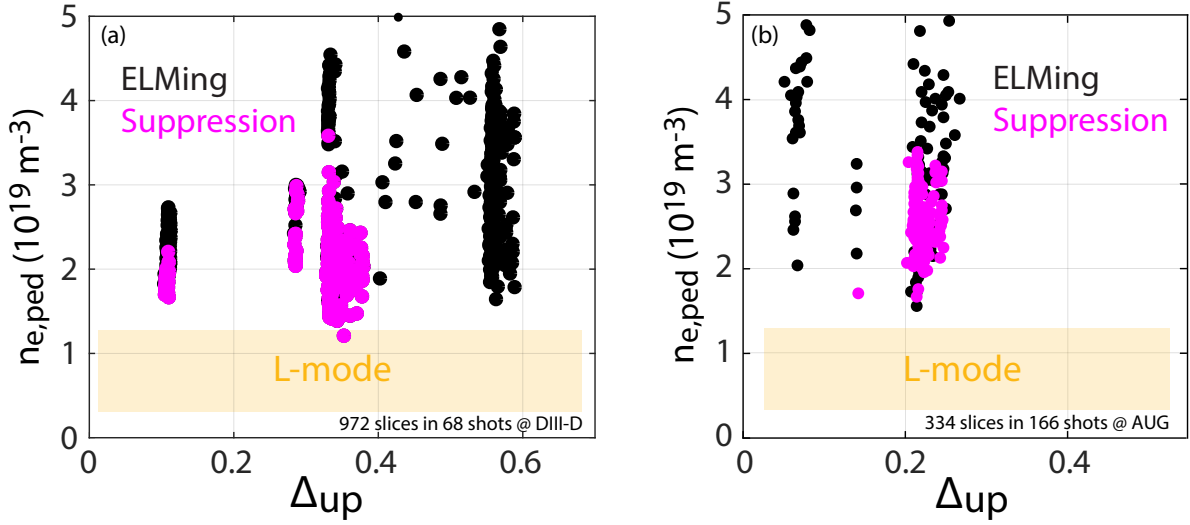


FIG. 1. Statistics of ELM suppression threshold with different triangularity in (a) DIII-D and (b) ASDEX Upgrade. The black points indicate ELM mitigation, the magenta points indicate ELM suppression.

resonant surfaces. It reveals that the resonant coupling is reduced at high triangularity as compared to that at low triangularity. This is validated through targeted comparisons with experiments at DIII-D, EAST, and ASDEX Upgrade, and can partially explain the experimental observations. Moreover, the multi-mode plasma response shows similar trends as the resonant coupling, implying that this provides another way to optimize RMP-ELM control.

The rest of this paper is structured as follows. Section II describes the experimental setup, along with the modeling approach used in this work. Section III describes modeling results in this work, and comparison with ELM control results in experiments. Section IV describes the validation between experiments and modeling. Section V describes the multi-modal analysis of the results, demonstrating that this technique provides another way to understand ELM control effects. Concluding remarks are given in section VI.

II. EXPERIMENTAL SETUP AND MODELING APPROACH

In this work, the plasma response to RMPs is systematically investigated by varying the axisymmetric plasma upper and lower triangularity, whilst keeping other equilibrium quanti-

ties largely unchanged or deliberately scanning them. Both experiments and simulations are performed in the investigation. The experiments are carried out in DIII-D, ASDEX Upgrade and EAST tokamaks with toroidal mode number $n = 3, 2, 1$ RMP applied, respectively. The simulation is carried out using the single-fluid linear resistive magneto-hydrodynamic (MHD) code MARS-F³⁰. Simulation results are used to evaluate the plasma response at different triangularity, while experimental results are used to verify the reliability of the simulation.

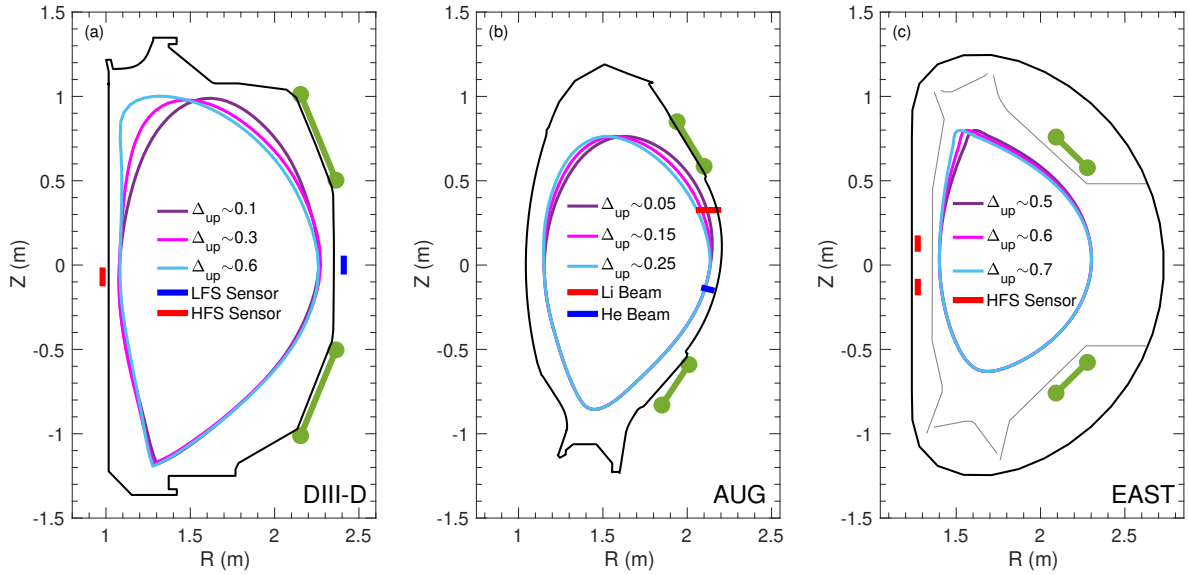


FIG. 2. Plasma shapes with different triangularity superimposed on the poloidal cross-section with RMP coils (green) and diagnostics (red, blue) used in this work in (a) DIII-D, (b) ASDEX Upgrade and (c) EAST.

The plasma shapes produced in experiments are shown in Figure 2. Lower single-null (LSN) plasma shapes are used in DIII-D and ASDEX Upgrade, while an upper single-null (USN) is used in EAST, the grad-B direction is into divertor for all shots in study. The upper triangularities are deliberately scanned in experiments for all three tokamaks. The triangularity Δ_{up} varies from 0.1 to 0.6 in DIII-D, from 0 to 0.3 in ASDEX Upgrade, and from 0.5 to 0.7 in EAST. The detailed experimental parameters are listed in Table I.

To preserve the influence of triangularity and exclude other factors, the equilibria used

TABLE I. Experimental parameters for the cases examined in this work.

Case	I_p (MA)	B_T (T)	q_{95}	β_N	n_{RMP}	Shape	Δ_{up}	Measurement
DIII-D	1.56	2.0	3.6	1.5~2.0	3	LSN	0.1~0.6	magnetic sensors
AUG	0.76	1.7	3.8	2.2	2	LSN	0~0.3	Li-Beam, He-Beam
EAST	0.37	2.2	5.9	0.5	1	USN	0.5~0.7	magnetic sensors

in the simulation are generated using two equilibrium codes. In order to reproduce the plasma response with different pedestal parameters, the equilibria of DIII-D are generated self-consistently using the SEGWAY³¹ code. Not only triangularity is scanned for the DIII-D case, but also the pedestal density $n_{e,ped}$ and the normalized beta β_N . Pedestal parameters in DIII-D are then calculated to be consistent with the EPED code predictions³². The equilibria of ASDEX Upgrade and EAST cases are generated using the CHEASE³³ code, and only triangularity is scanned in the process (without self-consistent pedestal prediction).

Targeted comparison of modeled plasma response with experiments is carried out in section IV. The high-field side (HFS) and low-field side (LFS) magnetic sensors in DIII-D and EAST allow validation on magnetic plasma response, while the lithium beam³⁴ (Li-Beam) and helium beam³⁵ (He-Beam) in ASDEX Upgrade allow validation on perturbed displacement. The location of these diagnostics are shown Figure 2.

III. CORRELATION OF THE CALCULATED PLASMA RESPONSE WITH ACCESS TO ELM SUPPRESSION

Previous studies found that the amplitude of edge resonant radial field component can be used to represent the plasma response that matters for ELM control^{36,37}. In this section, we choose the amplitude of edge resonant radial field component that near $\psi_p = 0.95$ surface $|b_{0.95}^{res}|$ as a metric to evaluate the influence of plasma shape in triangularity on plasma response and ELM control. Here, $b_{0.95}^{res} = (\frac{B^\rho}{B^\zeta})_{0.95}$, where B^ρ and B^ζ are the radial and toroidal components of magnetic fields in flux coordinate, the superscript *res* denotes the resonant component, the subscript 0.95 denotes the Fourier component with poloidal number m and toroidal number n of the m/n rational surface that is nearest to the $\psi_p = 0.95$ surface, and ψ_p denotes the normalized poloidal flux.

Comparison of plasma responses with different pedestal density $n_{e,ped}$ and normalized

beta β_N value is carried out for DIII-D $n = 3$ cases at $\delta\phi_{UL} = 0^\circ$. Here $\delta\phi_{UL}$ denotes the relative phase between upper and lower coil currents. One group is simulated using a set of low pedestal density equilibria ($n_{e,ped} \sim 2 \times 10^{19} m^{-3}$), the other group is simulated using a set of high pedestal density equilibria ($n_{e,ped} \sim 4 \times 10^{19} m^{-3}$). Both groups contain three β_N cases ($\beta_N \sim 1.5, 1.8, 2.0$) and vary the upper triangularity Δ_{up} from 0.1 to 0.6. These equilibria are generated self-consistently using the SEGWAY code³¹.

The edge resonant radial field component $|b_{0.95}^{res}|$ is simulated for these DIII-D cases, which is shown in Figure 3(a). The blue and red lines denote the plasma response at low and high pedestal density, respectively. The solid, dashed and dotted lines denote the plasma response at $\beta_N \sim 1.5, 1.8, 2.0$, respectively. It can be seen that the plasma response does not change much at low pedestal density for all β_N cases, which indicates the plasma response is insensitive to triangularity at low pedestal density. On the contrary, the plasma response is sensitive to triangularity at high pedestal density and high β_N . The resonance first increases with triangularity in the range of $\Delta_{up} \sim 0.1 - 0.2$, then decreases with it at $\Delta_{up} > 0.3$. The plasma response at low or moderate triangularity $\Delta_{up} \sim 0.1 - 0.4$ is obviously greater than that at high triangularity $\Delta_{up} \sim 0.4 - 0.6$.

These results are correlated with the experimental observations shown in Figure 1(a). The edge resonance of the high pedestal density case is greater at low or moderate triangularity $\Delta_{up} \sim 0.1 - 0.4$ as compared to that at high triangularity $\Delta_{up} \sim 0.4 - 0.6$. This agrees with the experimental results that ELMs cannot be suppressed at high triangularity. The edge resonance increases with triangularity in the range of $\Delta_{up} \sim 0.1 - 0.2$, also agreeing with the results that ELMs are easier to suppress at moderate triangularity as compared to low triangularity. Note that there is no experimental data at high pedestal density and low triangularity, and there is no ELM suppression at high $n_{e,ped} \sim 4 \times 10^{19} m^{-3}$ in experiment. The high pedestal density case in simulation are qualitatively compared to the ELM suppression observation in experiment. The simulation results can explain the degree of difficulty to access ELM suppression at different triangularities, while it cannot explain the density window of ELM suppression. These consistencies between experiment and simulation shows a correlation between the plasma response and ELM suppression access at different triangularities in DIII-D.

However, the simulation result cannot explain why ELM suppression is lost with density increases in experiment, because the linear response model is insufficient to simulate

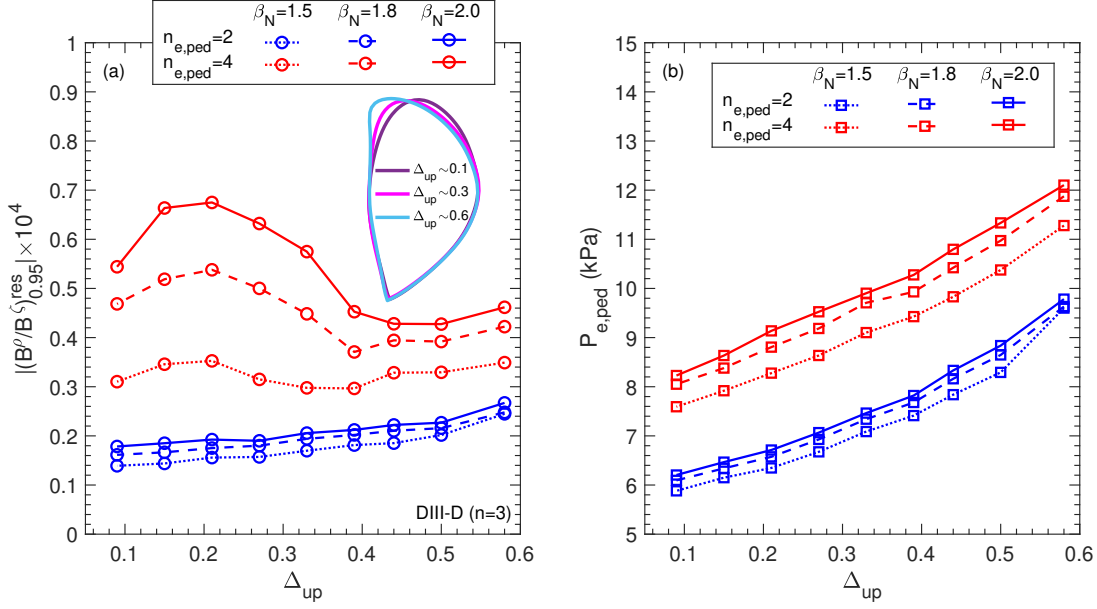


FIG. 3. (a) The amplitude of edge resonant radial field component near $\psi_p = 0.95$ surface simulated by the MARS-F code with $n = 3$ RMP applied at $\delta\phi_{UL} = 0^\circ$ in DIII-D. A sketch of plasma shapes of equilibria used in the simulation are superimposed on the figure. (b) The relation between pedestal pressure, pedestal density and triangularity of the equilibria used in MARS-F simulation. These equilibria are generated self-consistently using the SEGWAY code with the pedestal density $n_{e,\text{ped}} \sim 2 \times 10^{19} \text{m}^{-3}$ (blue), $4 \times 10^{19} \text{m}^{-3}$ (red) and $\beta_N \sim 1.5$ (dotted line), 1.8 (dashed line), 2.0 (solid line).

the transition between ELM suppression and mitigation¹⁸, and further non-linear model is required to understand the density effects on ELM control^{12,19}. Moreover, excessively low pedestal density in experiments lead to H-L back transitions, which is due to entirely different physics and is beyond the scope of this work. Thus the results of the low pedestal density limit cannot be verified through the experimental observations in this work.

We also point out that the density effect is not directly included in the MARS-F model. The DIII-D equilibria used in the simulation are generated self-consistently using the SEGWAY code³¹. When we scan the pedestal density, the pedestal pressure will change to keep the equilibria self-consistent with the EPED code pedestal predictions³². Figure 3(b) shows the pedestal pressure of the equilibria used in the simulation. The blue and red lines denote the low and high pedestal density, respectively. It can be seen that, to keep the equilibria

self-consistent with the EPED model, higher pedestal density would lead to higher pedestal pressure, which in turn cause more pressure driven edge response. Besides, the increase of pedestal pressure with triangularity also cancels out the reducing effect of triangularity on the plasma response to some extent, resulting in the slight increase of edge resonance at low pedestal density.

Similar modeling is carried out for ASDEX Upgrade with $n = 2$ RMP applied at $\delta\phi_{UL} = 0^\circ$ and EAST with $n = 1$ RMP applied under $\delta\phi_{UL}$ scan, which in accordance with that in experiments. The equilibria used in these cases are generated using the CHEASE³³ code, and the self-consistent pedestal evaluation was not available. The plasma shapes of those equilibria can be seen in Figure 4. The range of upper triangularity for ASDEX Upgrade is $\Delta_{up} \sim 0 - 0.3$, which corresponds to the range covered in experiments. The range of both upper and lower triangularity for EAST are extrapolated to $\Delta \sim 0.3 - 0.7$ in CHEASE³³, while only the upper triangularity is scanned in experiment from 0.5 to 0.7 (solid line). The reason of doing extrapolation for EAST equilibria is that the plasma shapes in EAST are USN, while those in DIII-D and ASDEX Upgrade are LSN. To ensure that same effects of triangularity are discussed in this work, both upper and lower triangularity are scanned for the EAST case in the simulation. This also explores the relative role of the triangularity of the X-point region as compared to the crown region.

Figure 4(a) shows the edge resonance for the ASDEX Upgrade case. It is calculated with $n = 2$ RMP applied at $\delta\phi_{UL} = 0^\circ$, which is the same as that in experiment. It can be seen that the resonance decreases with triangularity, which disagrees with the experimental observations shown in Figure 1(b), where ELMs are easier to be suppressed at $\Delta_{up} \sim 0.25$ in experiments. Figure 4(b) shows the peak value of edge resonance of the EAST case calculated under $\delta\phi_{UL}$ scan at each triangularity, which corresponds to the maximum plasma response at each triangularity. The red and blue line denote the resonance calculated in upper and lower triangularity scan, respectively. The solid line denotes that the equilibria used in simulation are interpolated from experiments, while the dashed line denotes that extrapolated from experiments. It can be seen that the edge resonance decreases with both upper and lower triangularity. The plasma response is sensitive to plasma shape at low triangularity, and insensitive at high triangularity. This is similar to the result of DIII-D high pedestal density case shown in Figure 3(a).

In summary, the simulated results in this section shows the influence of triangularity on

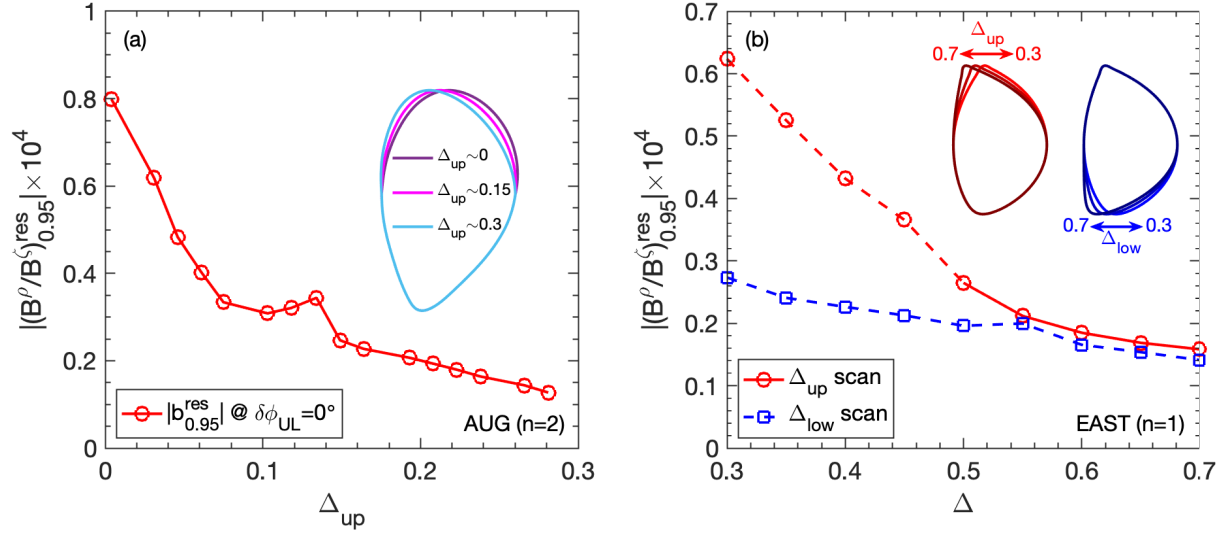


FIG. 4. (a) The amplitude of edge resonant radial field component near $\psi_p = 0.95$ surface simulated by the MARS-F code in ASDEX Upgrade with $n = 2$ RMP applied at $\delta\phi_{UL} = 0^\circ$, and (b) the peak value of that in EAST with $n = 1$ RMP applied under $\delta\phi_{UL}$ scan. A sketch of plasma shapes of equilibria used in the simulation are superimposed on these figures. These equilibria are generated with interpolation (solid line) and extrapolation (dashed line) from experimental equilibria using the CHEASE code.

the plasma response. The plasma response is sensitive to plasma shape in low triangularity and high pedestal density. This can partially explain the experimental observation shown in Figure 1 that ELM control effects is sensitive to triangularity and pedestal density. However, it cannot explain why the ELM suppression is lost with pedestal density increase, and why ELM suppression cannot be achieved at $\Delta_{\text{up}} \sim 0.1$ in ASDEX Upgrade. This also reveals the limitation in understanding ELM control only from the view of linear plasma response, further nonlinear models^{12,38} and 3D stability analysis³⁹ is required to better understand ELM control physics.

IV. DIAGNOSTICS ALLOW VALIDATION OF PLASMA RESPONSE SIMULATION

In order to test the reliability of the simulation, validation of plasma response between experiment and simulation is carried out. The validation involves all three tokamaks, and is discussed in this section.

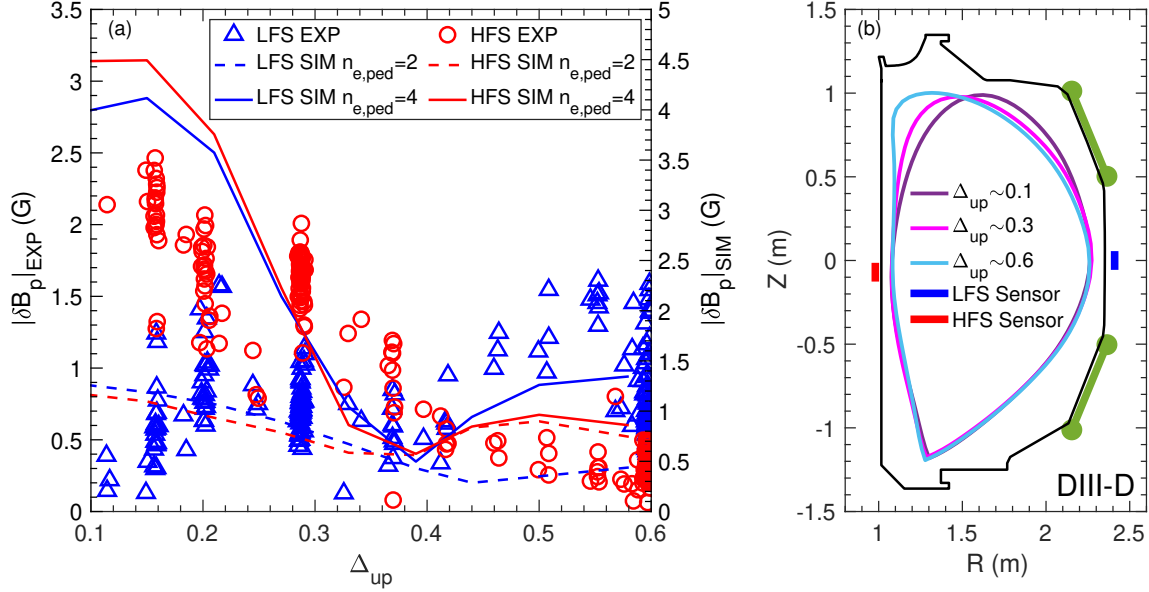


FIG. 5. (a) The measured (scatter markers) and simulated (dashed and solid lines) magnetic plasma response on LFS (blue) and HFS (red) at different triangularity in DIII-D, note that the left y-axis is for the measured plasma response and right y-axis is for the simulated one. (b) Locations of magnetic sensors superimposed on the poloidal cross-section with different plasma shapes in triangularity in DIII-D.

The magnetic diagnostics allow validation of the magnetic plasma response in DIII-D, the results of which are shown in Figure 5(a). The blue triangles and red circles denote the measured plasma response on LFS and HFS, respectively. The solid and dashed line denote the plasma response simulated with high and low pedestal density at $\beta_N \sim 1.8$. The location of the sensors on HFS and LFS are shown in Figure 5(b), as well as a diagram of plasma shape in different triangularity. It can be seen that the measured plasma response on the

HFS (red circles) decreases with triangularity, and the simulated high pedestal density result (red solid line) agrees with the measured one in trends, despite that the absolute value of the simulated plasma response is greater than the measured one. The measured plasma response on the LFS (blue triangles) is relatively flat, and the simulated low pedestal density result (blue dashed line) agrees with measured one at low triangularity, while the high pedestal density results (blue solid line) agrees with it at high triangularity. The parameter range of pedestal density and pedestal pressure in experiments are shown in Figure 6. The blue dots denote low triangularity cases ($\Delta_{up} < 0.2$), and the red dots denote high triangularity cases ($\Delta_{up} > 0.4$). There are no experimental points at low triangularity and high pedestal density, and the pedestal density for most experimental points at high triangularity is also high. Therefore, the LFS results in Figure 5(a) show good agreement between measurement and simulation, while the HFS results reproduce the trends with high pedestal density. In general, the simulated plasma response for DIII-D shows similar trends with measurement, which supports the modeling results presented in Section III.

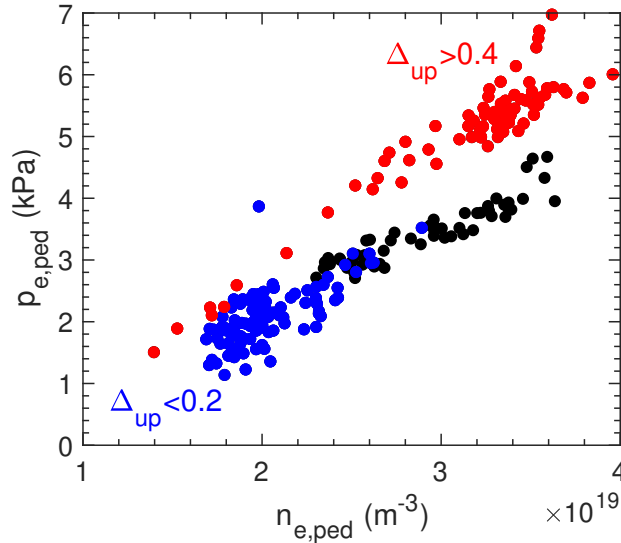


FIG. 6. Statistics of pedestal pressure and pedestal density in DIII-D experiments. The blue dots denote low triangularity cases ($\Delta_{up} < 0.2$), the black dots denote moderate triangularity cases ($0.2 < \Delta_{up} < 0.4$), the red dots denote high triangularity cases ($\Delta_{up} > 0.4$).

The magnetic sensors on EAST also allow validation of the plasma response simulation. Figure 7(a) shows the magnetic plasma response measured in EAST. The red, green and

blue markers denote the plasma response measured at triangularity $\Delta_{up} \sim 0.5$, 0.6 and 0.7, respectively. The red, green and blue lines are the corresponding simulated plasma response. The location of the magnetic sensors are shown in Figure 7(b). It can be seen that the plasma response measured on the HFS decreases with triangularity, and the $\delta\phi_{UL}$ dependence of the simulated plasma response agrees with the measured one, despite the fact that the absolute value is not captured in the simulation. Note that the simulated result in Figure 7(a) does not contradict the result in Figure 4(b), as the sensor measured plasma response is also affected by the location of measurement.

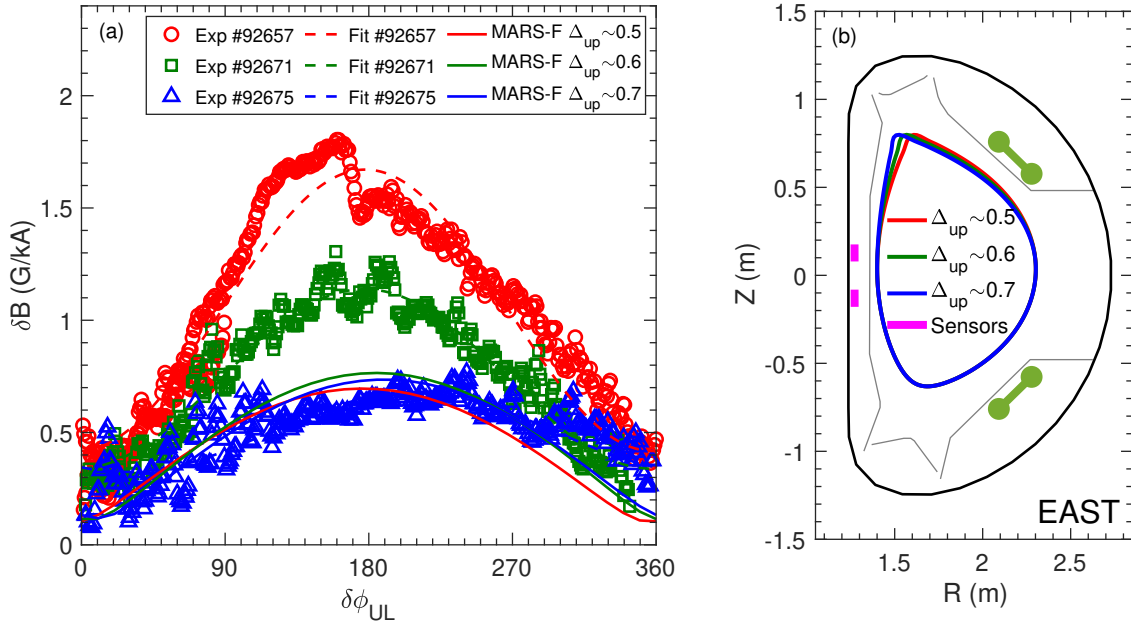


FIG. 7. (a) The measured (scatter markers) and simulated (solid lines) magnetic plasma response at different triangularity on HFS in EAST. (b) Locations of magnetic sensors superimposed on the poloidal cross-section with different plasma shapes in triangularity in EAST.

Unfortunately, no magnetic plasma response data is available on ASDEX Upgrade for this experiment. Instead, the perturbed displacement measured by the lithium beam and helium beam can be used to compare to the simulation results, which is shown in Figure 8 (a). The red circle and blue triangle denote the perturbed displacement measured by lithium beam and helium beam, respectively. The red solid line and blue dashed line denote the

simulated results. The position of these two diagnostics are shown in Figure 8(b). It can be seen that no clear trend is discernible in the measured data and the simulated displacement does not change much with triangularity, which implies that the perturbed displacement is insensitive to triangularity. The absolute value of the simulated perturbed displacement is within a factor of two, on average, with the measured one, which provides some confidence in the modeling results.

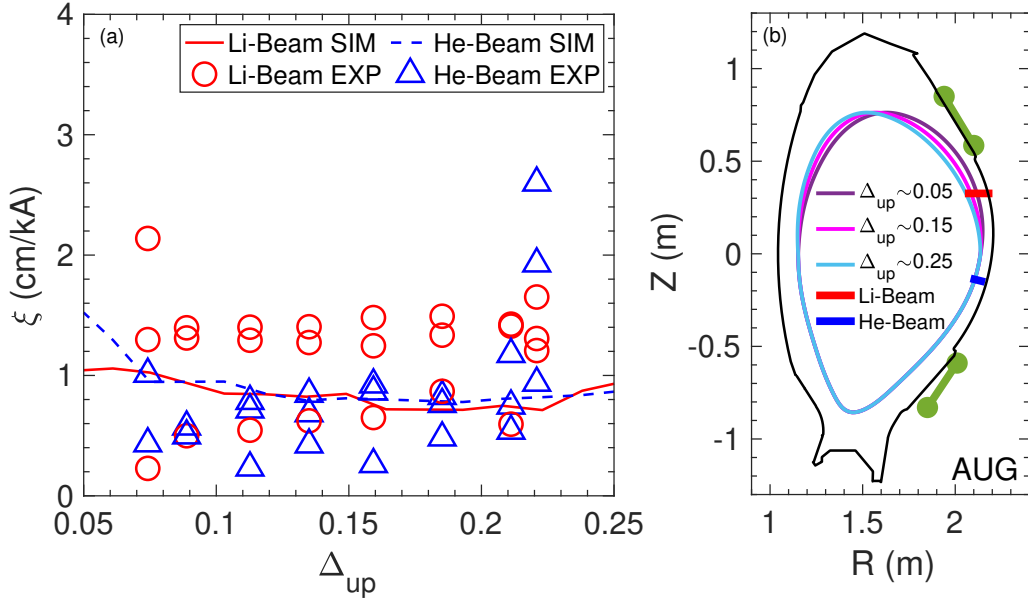


FIG. 8. (a) The perturbed displacement measured by the lithium beam (red circle) and helium beam (blue triangle) in ASDEX Upgrade, as well as the corresponding simulated ones (red solid line and blue dashed line). (b) Locations of perturbed displacement measured by the lithium beam (red solid line) and helium beam (blue solid line), as well as a diagram of plasma shapes with different triangularity in ASDEX Upgrade.

In summary, the measured and simulated magnetic plasma response reveals similar trends, and the HFS magnetic plasma response decreases with triangularity. The simulated perturbed displacement at LFS mid-plane agrees well with the measurement in ASDEX Upgrade, and it is insensitive to triangularity. The agreement between experiment and simulation indicates the reliability of the linear plasma response model.

V. ADDITIONAL UNDERSTANDING ENABLED BY DYNAMIC EVOLUTION OF THE MULTI-MODE PLASMA RESPONSE

Previous studies found that the plasma response is multi-modal^{20,22,24,40}, and several methods were proposed to extract the multi-mode plasma response^{20,21,24,41}. In this section, multi-modal analysis for plasma response is carried out using the method presented in Ref [24].

For completeness, the method is briefly summarized here. The singular value decomposition (SVD) technique is used to extract the multi-mode plasma response. It is a factorization of a complex matrix \mathbf{A} , as $\mathbf{A} = \mathbf{U}\mathbf{S}\mathbf{V}^*$. Here, the complex matrix \mathbf{A} contains data about mode amplitude and phase, with each row the spatial structure of the plasma response and each column the $\delta\phi_{UL}$ dependence of the plasma response. After the decomposition, the right-singular vectors $V_{\#i}$ (columns of \mathbf{V}) form a set of orthonormal basis vectors for the spatial structure of each mode. The left-singular vectors $U_{\#i}$ (columns of \mathbf{U}) form an orthonormal basis for the dependence on $\delta\phi_{UL}$ of each mode. Each element $S_{\#i}$ on the diagonal of \mathbf{S} represents the amplitude or the eigenvalue of the mode identified by $V_{\#i}$ and $U_{\#i}$, and the square of it $S_{\#i}^2$ denotes the energy of the mode.

Figure 9 shows the mode structure of the dominant and secondary mode extracted using SVD for DIII-D case at low triangularity $\Delta_{up} \sim 0.1$ and high triangularity $\Delta_{up} \sim 0.6$. It can be seen that the mode structure at high and low triangularity are similar, as the dominant modes are both stronger near the X-point and weaker on mid-plane, while the secondary modes are both stronger on LFS mid-plane. The similarity of mode structure suggests that it does not change with triangularity. The $\delta\phi_{UL}$ dependence of these modes are shown in Figure 10. The red solid line denotes the dominant mode and the blue dashed line denotes the secondary mode. Figure 10(a) shows the results at low triangularity $\Delta_{up} \sim 0.1$, while Figure 10(b) for high triangularity $\Delta_{up} \sim 0.6$. It can be seen that the $\delta\phi_{UL}$ dependence of these modes are similar at both high and low triangularity, which further supports the conclusion that the mode does not change with triangularity. Similar results are found in the ASDEX Upgrade and EAST cases indicating that the structure and $\delta\phi_{UL}$ dependence of multi-mode plasma response do not change with triangularity.

However, the eigenvalue S_i of the multi-mode plasma response does change with triangularity, as shown in Figure 11 (a). The red lines denote the dominant mode and the blue lines

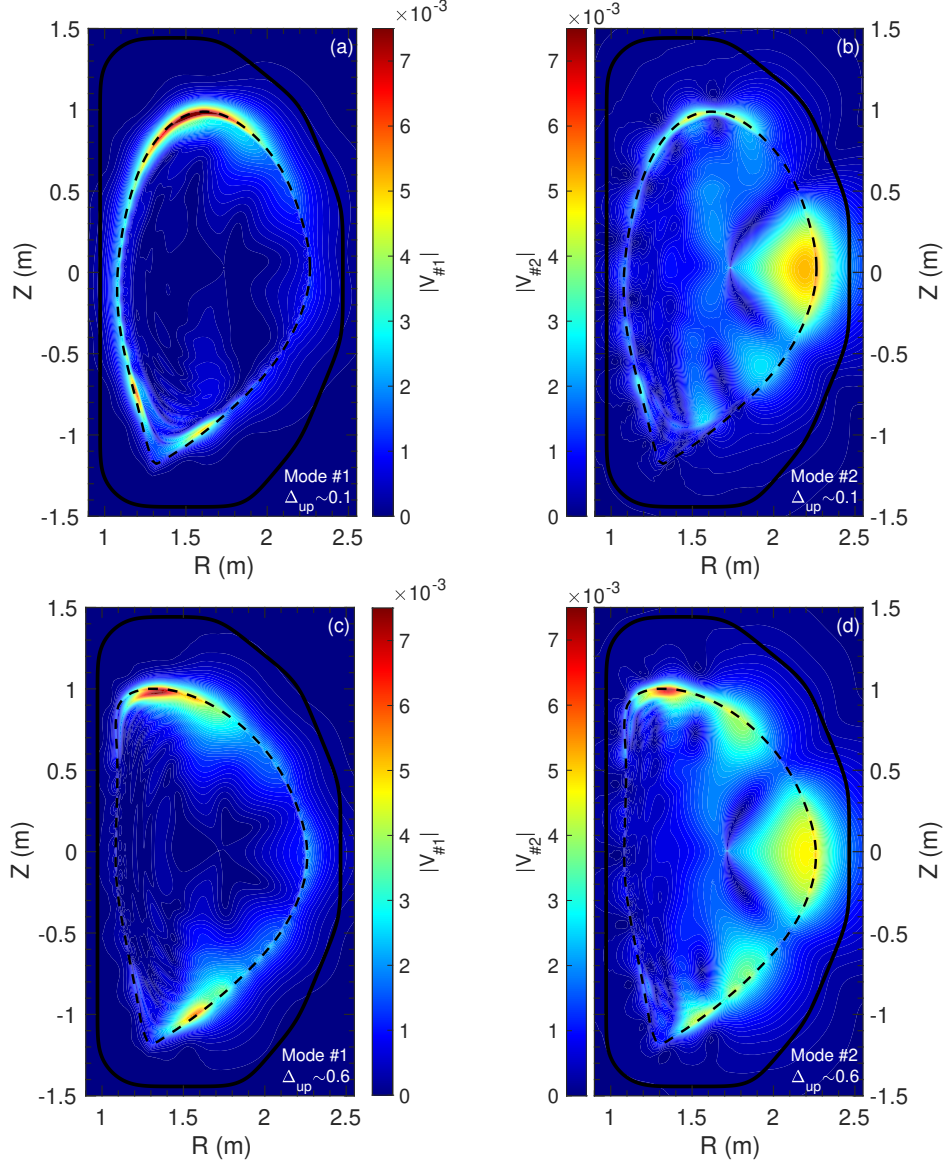


FIG. 9. Mode structure of B_r components of the (a,c) dominant and (b,d) secondary mode at (a,b) low triangularity $\Delta_{up} \sim 0.1$ and (b,d) high triangularity $\Delta_{up} \sim 0.6$ in DIII-D.

denote the secondary mode. It can be seen that the amplitude of the dominant mode at low or moderate triangularity $\Delta_{up} < 0.4$ is greater than that at high triangularity $\Delta_{up} > 0.4$. This reveals similar trends with the results presented in Figure 3 (a). It also can be used to explain the experimental observations shown in Figure 1(a), that the mode associated with ELM control effect is stronger at low or moderate triangularity, thus ELM suppression is easier to be achieved at this regime.

Previous studies show that the edge kink-peeling response is a key indicator for the

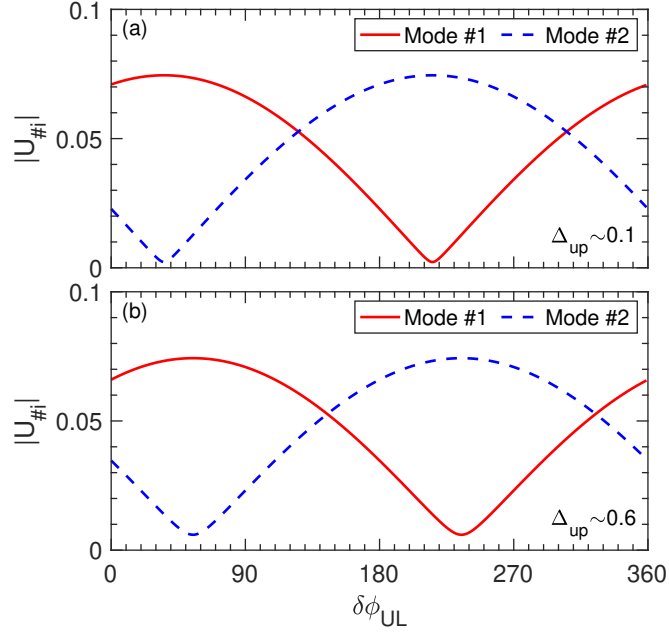


FIG. 10. The computed $\delta\phi_{UL}$ dependence of the dominant (red solid line) and secondary (blue dashed line) modes at (a) low triangularity $\Delta_{up} \sim 0.1$ and (b) high triangularity $\Delta_{up} \sim 0.6$ in DIII-D.

effect of ELM control¹¹. Several parameters can be used as metrics for the edge kink-peeling response, such as the amplitude of edge resonant radial field component $|b^{res}|$ ^{36,37}, and the amplitude of radial displacement near X-point $|\xi_X|$ ⁴². As far as the linear resistive plasma response is concerned, these metrics are co-linear and reveal similar results in finding the optimal coil phasing for ELM control^{24,43}. Figure 11(b) shows the amplitude of radial displacement near X-point $|\xi_X|$, which is another metric that can be used to evaluate the plasma response for ELM control⁴². It can be seen that the displacement near X-point at low or moderate triangularity $\Delta_{up} < 0.4$ is much greater than that at high triangularity $\Delta_{up} > 0.4$, which also agrees with the experimental observation. Indeed, the X-point displacement appears to decay more strongly with triangularity than the resonant fields.

The dominant mode of multi-mode plasma response reveals similar trends with the edge resonance and the radial displacement near X-point, and all these three metrics show agreement with experimental observations. It implies that the dynamic evolution of the multi-mode plasma response provides another way to understand the ELM control physics.

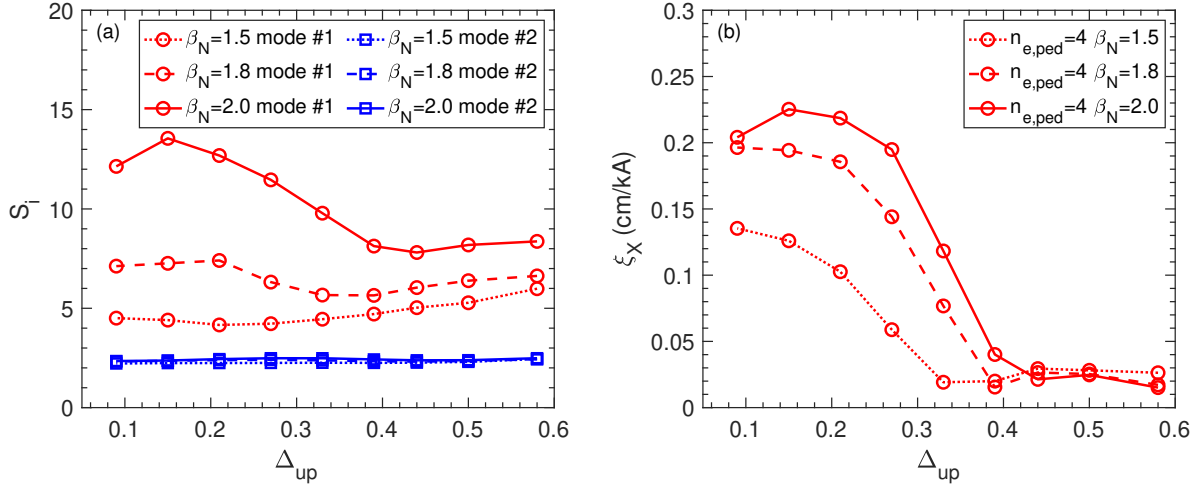


FIG. 11. (a) The eigenvalue of the dominant (red) and secondary (blue) mode at pedestal density $n_{e,ped} \sim 4 \times 10^{19} m^{-3}$ and $\beta_N \sim 1.5$ (dotted line), 1.8 (dashed line) and 2.0 (solid line) in DIII-D. (b) The perturbed radial displacement near X-point of these cases in DIII-D.

VI. CONCLUSION

In conclusion, the influence of plasma shape in triangularity on plasma response to RMPs is investigated for the DIII-D, EAST and ASDEX Upgrade tokamaks in this work. In general, the magnetic plasma response decreases with triangularity in both resonant harmonics and HFS sensor measurements. The plasma response is sensitive to plasma shape at low triangularity, while the sensitivity decreases at high triangularity. The resonance of plasma response is correlated with ELM suppression access, and can be used to partially explain the ELM control effects in DIII-D. The ASDEX Upgrade results indicating improved access at low triangularity, however, are not explained.

Comparison of experimental measurements and modeling results shows agreement in trends on DIII-D and EAST. This suggests that the magnetic plasma response can be well simulated in the linear model. The agreement of the amplitude of perturbed displacement on LFS mid-plane between experiment and modeling in ASDEX Upgrade further proves this point, despite that it is insensitive to triangularity.

Multi-modal analysis of the simulation results extracts the mode structure and applied spectrum dependence of each mode. The amplitude of the dominant mode shows similar

trends as the edge resonance and X-point displacement. This suggests that dynamic evolution of multi-mode plasma response provides another way to understand the ELM control physics.

However, the linear MHD model still has limitations in modeling ELM suppression access, as it cannot explain, for example, why ELM suppression is lost with pedestal density increase. Besides, the simulation results also disagree with the fact that no ELM suppression has been achieved in ASDEX Upgrade at $\Delta_{up} \sim 0.1$ yet, which implies that it is insufficient to understand ELM control only from the view of the plasma response. Further nonlinear MHD¹² and 3D stability analysis³⁹ is required for better understanding ELM control in experiment.

The plasma response is strongly reduced at high triangularity compared to that at low triangularity, which implies different control effects of RMPs as the plasma shape is varied. These results indicate that the plasma shape should be taken into consideration when designing a tokamak suitable for RMP-ELM control, and that predictive plasma response calculations can be used to maximize access to RMP-ELM control in future devices by maximizing the coupling between the coils and the plasma^{44,45}.

ACKNOWLEDGMENT

This work is supported by US DOE under DE-SC0020298, DE-SC0021968, DE-FC02-04ER54698, DE-AC52-07NA27344, DE-AC02-09CH11466, DE-SC0022270, DE-AC05-00OR22725. This work is supported by the National Key R&D Program of China under Grant No. 2017YFE0301100 and the National Natural Science Foundation of China under Grant Nos. 11875292 and 11805237. This work has been carried out within the framework of the EUROfusion Consortium and has received funding from the Euratom research and training programme 2014-2018 and 2019-2020 under grant agreement number 633053. The views and opinions expressed herein do not necessarily reflect those of the European Commission. C. Paz-Soldan acknowledges consulting for General Atomics.

DISCLAIMER

This report was prepared as an account of work sponsored by an agency of the United States Government. Neither the United States Government nor any agency thereof, nor any of their employees, makes any warranty, express or implied, or assumes any legal liability or responsibility for the accuracy, completeness, or usefulness of any information, apparatus, product, or process disclosed, or represents that its use would not infringe privately owned rights. Reference herein to any specific commercial product, process, or service by trade name, trademark, manufacturer, or otherwise, does not necessarily constitute or imply its endorsement, recommendation, or favoring by the United States Government or any agency thereof. The views and opinions of authors expressed herein do not necessarily state or reflect those of the United States Government or any agency thereof.

REFERENCES

- ¹T. E. Evans, Resonant magnetic perturbations of edge-plasmas in toroidal confinement devices, *Plasma Physics and Controlled Fusion* 57 (2015) 123001. URL: <http://dx.doi.org/10.1088/0741-3335/57/12/123001>. doi:doi:10.1088/0741-3335/57/12/123001.
- ²A. Loarte, G. Huijsmans, S. Futatani, L. Baylor, T. Evans, D. M. Orlov, O. Schmitz, M. Becoulet, P. Cahyna, Y. Gribov, A. Kavin, A. Sashala Naik, D. Campbell, T. Casper, E. Daly, H. Frerichs, A. Kischner, R. Laengner, S. Lisgo, R. Pitts, G. Saibene, A. Wingen, Progress on the application of ELM control schemes to ITER scenarios from the non-active phase to DT operation, *Nuclear Fusion* 54 (2014) 033007. URL: <http://dx.doi.org/10.1088/0029-5515/54/3/033007>. doi:doi:10.1088/0029-5515/54/3/033007.
- ³T. E. Evans, R. A. Moyer, P. R. Thomas, J. G. Watkins, T. H. Osborne, J. A. Boedo, E. J. Doyle, M. E. Fenstermacher, K. H. Finken, R. J. Groebner, M. Groth, J. H. Harris, R. J. La Haye, C. J. Lasnier, S. Masuzaki, N. Ohyabu, D. G. Pretty, T. L. Rhodes, H. Reimerdes, D. L. Rudakov, M. J. Schaffer, G. Wang, L. Zeng, Suppression of Large Edge-Localized Modes in High-Confinement DIII-D Plasmas with a Stochastic Magnetic Boundary, *Physical Review Letters* 92 (2004) 235003. URL: <http://dx.doi.org/10.1103/PhysRevLett.92.235003>. doi:doi:10.1103/PhysRevLett.92.235003.

- ⁴Y. Liang, H. R. Koslowski, P. R. Thomas, E. Nardon, B. Alper, P. Andrew, Y. Andrew, G. Arnoux, Y. Baranov, M. Bécoulet, M. Beurskens, T. Biewer, M. Bigi, K. Crombe, E. De La Luna, P. De Vries, W. Fundamenski, S. Gerasimov, C. Giroud, M. P. Gryaznevich, N. Hawkes, S. Hotchin, D. Howell, S. Jachmich, V. Kiptily, L. Moreira, V. Parail, S. D. Pinches, E. Rachlew, O. Zimmermann, Active control of type-I edge-localized modes with $n=1$ perturbation fields in the JET tokamak, *Physical Review Letters* 98 (2007) 265004. URL: <http://dx.doi.org/10.1103/PhysRevLett.98.265004>. doi:doi:10.1103/PhysRevLett.98.265004.
- ⁵A. Kirk, Y. Liu, E. Nardon, P. Tamain, P. Cahyna, I. Chapman, P. Denner, H. Meyer, S. Mordijck, D. Temple, Magnetic perturbation experiments on MAST L- and H-mode plasmas using internal coils, *Plasma Physics and Controlled Fusion* 53 (2011) 065011. URL: <https://doi.org/10.1088/0741-3335/53/6/065011>. doi:doi:10.1088/0741-3335/53/6/065011.
- ⁶W. Suttrop, T. Eich, J. C. Fuchs, S. Günter, A. Janzer, A. Herrmann, A. Kallenbach, P. T. Lang, T. Lunt, M. Maraschek, R. M. McDermott, A. Mlynec, T. Pütterich, M. Rott, T. Vierle, E. Wolfrum, Q. Yu, I. Zammuto, H. Zohm, First Observation of Edge Localized Modes Mitigation with Resonant and Nonresonant Magnetic Perturbations in ASDEX Upgrade, *Physical Review Letters* 106 (2011) 225004. URL: <http://dx.doi.org/10.1103/PhysRevLett.106.225004>. doi:doi:10.1103/PhysRevLett.106.225004.
- ⁷Y. M. Jeon, J.-K. Park, S. W. Yoon, W. H. Ko, S. G. Lee, K. D. Lee, G. S. Yun, Y. U. Nam, W. C. Kim, J.-G. Kwak, K. S. Lee, H. K. Kim, H. L. Yang, Suppression of Edge Localized Modes in High-Confinement KSTAR Plasmas by Nonaxisymmetric Magnetic Perturbations, *Physical Review Letters* 109 (2012) 035004. URL: <http://dx.doi.org/10.1103/PhysRevLett.109.035004>. doi:doi:10.1103/PhysRevLett.109.035004.
- ⁸Y. Sun, Y. Liang, Y. Q. Liu, S. Gu, X. Yang, W. Guo, T. Shi, M. Jia, L. Wang, B. Lyu, C. Zhou, A. Liu, Q. Zang, H. Liu, N. Chu, H. H. Wang, T. Zhang, J. Qian, L. Xu, K. He, D. Chen, B. Shen, X. Gong, X. Ji, S. Wang, M. Qi, Y. Song, Q. Yuan, Z. Sheng, G. Gao, P. Fu, B. Wan, Nonlinear Transition from Mitigation to Suppression of the Edge Localized Mode with Resonant Magnetic Perturbations in the EAST Tokamak, *Physical Review Letters* 117 (2016) 115001. URL: <http://dx.doi.org/10.1103/PhysRevLett.117.115001>. doi:doi:10.1103/PhysRevLett.117.115001.

- ⁹T. F. Sun, Y. Liu, X. Q. Ji, Y. Q. Liu, R. Ke, J. M. Gao, N. Wu, W. Deng, M. Xu, X. R. Duan, Edge-coherent oscillation providing nearly continuous transport during edge-localized mode mitigation by $n = 1$ resonant magnetic perturbation in HL-2A, *Nuclear Fusion* 61 (2021) 036020. URL: <http://dx.doi.org/10.1088/1741-4326/abd2c7>. doi:doi:10.1088/1741-4326/abd2c7.
- ¹⁰A. Kirk, W. Suttrop, I. Chapman, Y. Liu, R. Scannell, A. Thornton, L. B. Orte, P. Cahyna, T. Eich, R. Fischer, C. Fuchs, C. Ham, J. Harrison, M. Jakubowski, B. Kurzan, S. Pamela, M. Peterka, D. Ryan, S. Saarelma, B. Sieglin, M. Valovic, M. Willensdorfer, Effect of resonant magnetic perturbations on low collisionality discharges in MAST and a comparison with ASDEX Upgrade, *Nuclear Fusion* 55 (2015) 043011. URL: <http://dx.doi.org/10.1088/0029-5515/55/4/043011>. doi:doi:10.1088/0029-5515/55/4/043011.
- ¹¹Y. Liu, C. J. Ham, A. Kirk, L. Li, A. Loarte, D. A. Ryan, Y. Sun, W. Suttrop, X. Yang, L. Zhou, ELM control with RMP: plasma response models and the role of edge peeling response, *Plasma Physics and Controlled Fusion* 58 (2016) 114005. URL: <http://dx.doi.org/10.1088/0741-3335/58/11/114005>. doi:doi:10.1088/0741-3335/58/11/114005. [arXiv:1607.01161](https://arxiv.org/abs/1607.01161).
- ¹²Q. M. Hu, R. Nazikian, B. A. Grierson, N. C. Logan, C. Paz-Soldan, Q. Yu, The role of edge resonant magnetic perturbations in edge-localized-mode suppression and density pump-out in low-collisionality DIII-D plasmas, *Nuclear Fusion* 60 (2020) 076001. URL: <http://dx.doi.org/10.1088/1741-4326/ab8545>. doi:doi:10.1088/1741-4326/ab8545.
- ¹³Y. Liu, A. Kirk, Y. Gribov, M. Gryaznevich, T. Hender, E. Nardon, Modelling of plasma response to resonant magnetic perturbation fields in MAST and ITER, *Nuclear Fusion* 51 (2011) 083002. URL: <http://dx.doi.org/10.1088/0029-5515/51/8/083002>. doi:doi:10.1088/0029-5515/51/8/083002.
- ¹⁴B. C. Lyons, N. M. Ferraro, C. Paz-Soldan, R. Nazikian, A. Wingen, Effect of rotation zero-crossing on single-fluid plasma response to three-dimensional magnetic perturbations, *Plasma Physics and Controlled Fusion* 59 (2017) 044001. URL: <http://dx.doi.org/10.1088/1361-6587/aa5860>. doi:doi:10.1088/1361-6587/aa5860.
- ¹⁵Z. R. Wang, M. J. Lanctot, Y. Q. Liu, J. K. Park, J. E. Menard, Three-dimensional drift kinetic response of high- β plasmas in the DIII-D tokamak, *Physical Review Letters* 114 (2015) 145005. URL: <http://dx.doi.org/10.1103/PhysRevLett.114.145005>. doi:doi:10.1103/PhysRevLett.114.145005.

- ¹⁶C. Paz-Soldan, N. Logan, S. Haskey, R. Nazikian, E. Strait, X. Chen, N. Ferraro, J. King, B. Lyons, J.-K. Park, Equilibrium drives of the low and high field side $n = 2$ plasma response and impact on global confinement, *Nuclear Fusion* 56 (2016) 056001. URL: <http://dx.doi.org/10.1088/0029-5515/56/5/056001>. doi:doi:10.1088/0029-5515/56/5/056001.
- ¹⁷R. Nazikian, C. Paz-Soldan, J. D. Callen, J. S. DeGrassie, D. Eldon, T. E. Evans, N. M. Ferraro, B. A. Grierson, R. J. Groebner, S. R. Haskey, C. C. Hegna, J. D. King, N. C. Logan, G. R. McKee, R. A. Moyer, M. Okabayashi, D. M. Orlov, T. H. Osborne, J.-K. Park, T. L. Rhodes, M. W. Shafer, P. B. Snyder, W. M. Solomon, E. J. Strait, M. R. Wade, Pedestal Bifurcation and Resonant Field Penetration at the Threshold of Edge-Localized Mode Suppression in the DIII-D Tokamak, *Physical Review Letters* 114 (2015) 105002. URL: <http://dx.doi.org/10.1103/PhysRevLett.114.105002>. doi:doi:10.1103/PhysRevLett.114.105002.
- ¹⁸S. Gu, Y. Sun, C. Paz-Soldan, R. Nazikian, M. Jia, H. Wang, W. Guo, Y. Liu, T. Abrams, L. Cui, T. Evans, A. Garofalo, X. Gong, N. Logan, S. Munaretto, D. Orlov, T. Shi, Edge localized mode suppression and plasma response using mixed toroidal harmonic resonant magnetic perturbations in DIII-D, *Nuclear Fusion* 59 (2019) 026012. URL: <http://dx.doi.org/10.1088/1741-4326/aaf5a3>. doi:doi:10.1088/1741-4326/aaf5a3.
- ¹⁹Q. M. Hu, R. Nazikian, B. A. Grierson, N. C. Logan, D. M. Orlov, C. Paz-Soldan, Q. Yu, Wide Operational Windows of Edge-Localized Mode Suppression by Resonant Magnetic Perturbations in the DIII-D Tokamak, *Physical Review Letters* 125 (2020) 045001. URL: <http://dx.doi.org/10.1103/PhysRevLett.125.045001>. doi:doi:10.1103/PhysRevLett.125.045001. [arXiv:1912.06555](https://arxiv.org/abs/1912.06555).
- ²⁰C. Paz-Soldan, R. Nazikian, S. R. Haskey, N. C. Logan, E. J. Strait, N. M. Ferraro, J. M. Hanson, J. D. King, M. J. Lanctot, R. A. Moyer, M. Okabayashi, J.-K. Park, M. W. Shafer, B. J. Tobias, Observation of a Multimode Plasma Response and its Relationship to Density Pumpout and Edge-Localized Mode Suppression, *Physical Review Letters* 114 (2015) 105001. URL: <http://dx.doi.org/10.1103/PhysRevLett.114.105001>. doi:doi:10.1103/PhysRevLett.114.105001.
- ²¹N. C. Logan, C. Paz-Soldan, J.-K. Park, R. Nazikian, Identification of multi-modal plasma responses to applied magnetic perturbations using the plasma reluctance, *Physics of Plasmas* 23 (2016) 056110. URL: <http://dx.doi.org/10.1063/1.4948281>. doi:doi:

10.1063/1.4948281.

- ²²N. Logan, L. Cui, H. Wang, Y. Sun, S. Gu, G. Li, R. Nazikian, C. Paz-Soldan, Magnetic polarization measurements of the multi-modal plasma response to 3D fields in the EAST tokamak, *Nuclear Fusion* 58 (2018) 076016. URL: <http://dx.doi.org/10.1088/1741-4326/aac129>. doi:doi:10.1088/1741-4326/aac129.
- ²³J. K. Park, Y. M. Jeon, Y. In, J. W. Ahn, R. Nazikian, G. Park, J. Kim, H. H. Lee, W. H. Ko, H. S. Kim, N. C. Logan, Z. Wang, E. A. Feibush, J. E. Menard, M. C. Zarnstroff, 3D field phase-space control in tokamak plasmas, *Nature Physics* 14 (2018) 1223–1228. URL: <http://dx.doi.org/10.1038/s41567-018-0268-8>. doi:doi:10.1038/s41567-018-0268-8.
- ²⁴S. Gu, B. Wan, Y. Sun, N. Chu, Y. Liu, T. Shi, H. Wang, M. Jia, K. He, A new criterion for controlling edge localized modes based on a multi-mode plasma response, *Nuclear Fusion* 59 (2019) 126042. URL: <http://dx.doi.org/10.1088/1741-4326/ab4566>. doi:doi:10.1088/1741-4326/ab4566.
- ²⁵B. Hudson, T. Evans, C. Petty, P. Snyder, Dependence of resonant magnetic perturbation experiments on the DIII-D plasma shape, *Nuclear Fusion* 50 (2010) 064005. URL: <http://dx.doi.org/10.1088/0029-5515/50/6/064005>. doi:doi:10.1088/0029-5515/50/6/064005.
- ²⁶Y. Liu, B. C. Lyons, S. Gu, A. Kirk, L. Li, C. Paz-Soldan, M. W. Shafer, A. D. Turnbull, Influence of up-down asymmetry in plasma shape on RMP response, *Plasma Physics and Controlled Fusion* 63 (2021) 065003. URL: <http://dx.doi.org/10.1088/1361-6587/abf572>. doi:doi:10.1088/1361-6587/abf572.
- ²⁷C. Paz-Soldan, R. Nazikian, L. Cui, B. C. Lyons, D. M. Orlov, A. Kirk, N. C. Logan, T. H. Osborne, W. Suttrop, D. B. Weisberg, The effect of plasma shape and neutral beam mix on the rotation threshold for RMP-ELM suppression, *Nuclear Fusion* 59 (2019) 056012. URL: <http://dx.doi.org/10.1088/1741-4326/ab04c0>. doi:doi:10.1088/1741-4326/ab04c0.
- ²⁸W. Suttrop, A. Kirk, R. Nazikian, N. Leuthold, E. Strumberger, M. Willensdorfer, M. Cavedon, M. Dunne, R. Fischer, S. Fietz, J. C. Fuchs, Y. Q. Liu, R. M. McDermott, F. Orain, D. A. Ryan, E. Viezzer, Experimental studies of high-confinement mode plasma response to non-axisymmetric magnetic perturbations in ASDEX Upgrade, *Plasma Physics and Controlled Fusion* 59 (2017) 014049. URL: <http://dx.doi.org/10.1088/0741-3335/59/1/014049>. doi:doi:10.1088/0741-3335/59/1/014049.

- ²⁹X. Yang, Y. Liu, W. Xu, Y. He, S. Lu, Influence of elongation and triangularity on plasma response to resonant magnetic perturbations, *Nuclear Fusion* 62 (2022) 016013. URL: <http://dx.doi.org/10.1088/1741-4326/ac2636>. doi:doi:10.1088/1741-4326/ac2636.
- ³⁰Y. Liu, A. Kirk, E. Nardon, Full toroidal plasma response to externally applied nonaxisymmetric magnetic fields, *Physics of Plasmas* 17 (2010) 122502. URL: <http://dx.doi.org/10.1063/1.3526677>. doi:doi:10.1063/1.3526677.
- ³¹B. C. Lyons, C. Paz-Soldan, O. Meneghini, L. L. Lao, D. B. Weisberg, E. A. Belli, T. E. Evans, N. M. Ferraro, P. B. Snyder, Predict-first experimental analysis using automated and integrated magnetohydrodynamic modeling, *Physics of Plasmas* 25 (2018) 056111. URL: <http://dx.doi.org/10.1063/1.5025838>. doi:doi:10.1063/1.5025838.
- ³²P. B. Snyder, T. H. Osborne, K. H. Burrell, R. J. Groebner, A. W. Leonard, R. Nazikian, D. M. Orlov, O. Schmitz, M. R. Wade, H. R. Wilson, The EPED pedestal model and edge localized mode-suppressed regimes: Studies of quiescent H-mode and development of a model for edge localized mode suppression via resonant magnetic perturbations, *Physics of Plasmas* 19 (2012) 056115. URL: <http://dx.doi.org/10.1063/1.3699623>. doi:doi:10.1063/1.3699623.
- ³³H. Lütjens, A. Bondeson, O. Sauter, The CHEASE code for toroidal MHD equilibria, *Computer Physics Communications* 97 (1996) 219–260. URL: [http://dx.doi.org/10.1016/0010-4655\(96\)00046-X](http://dx.doi.org/10.1016/0010-4655(96)00046-X). doi:doi:10.1016/0010-4655(96)00046-X.
- ³⁴M. Willensdorfer, G. Birkenmeier, R. Fischer, F. M. Laggner, E. Wolfrum, G. Veres, F. Aumayr, D. Carralero, L. Guimarães, B. Kurzan, Characterization of the Li-BES at ASDEX Upgrade, *Plasma Physics and Controlled Fusion* 56 (2014) 025008. URL: <http://dx.doi.org/10.1088/0741-3335/56/2/025008>. doi:doi:10.1088/0741-3335/56/2/025008.
- ³⁵M. Griener, J. M. Burgos, M. Cavedon, G. Birkenmeier, R. Dux, B. Kurzan, O. Schmitz, B. Sieglin, U. Stroth, E. Viezzer, E. Wolfrum, Qualification and implementation of line ratio spectroscopy on helium as plasma edge diagnostic at ASDEX Upgrade, *Plasma Physics and Controlled Fusion* 60 (2018) 025008. URL: <http://dx.doi.org/10.1088/1361-6587/aa97e8>. doi:doi:10.1088/1361-6587/aa97e8.
- ³⁶X. Yang, Y. Sun, Y. Liu, S. Gu, Y. Liu, H. Wang, L. Zhou, W. Guo, Modelling of plasma response to 3D external magnetic field perturbations in EAST, *Plasma Physics and Controlled Fusion* 58 (2016) 114006. URL: <http://dx.doi.org/10.1088/0741-3335/58/11/114006>. doi:doi:10.1088/0741-3335/58/11/114006.

- ³⁷L. Li, Y. Liu, A. Kirk, N. Wang, Y. Liang, D. Ryan, W. Suttrop, M. Dunne, R. Fischer, J. Fuchs, B. Kurzan, P. Piovesan, M. Willensdorfer, F. Zhong, Modelling plasma response to RMP fields in ASDEX Upgrade with varying edge safety factor and triangularity, *Nuclear Fusion* 56 (2016) 126007. URL: <http://dx.doi.org/10.1088/0029-5515/56/12/126007>. doi:doi:10.1088/0029-5515/56/12/126007.
- ³⁸N. C. Logan, J. K. Park, Q. Hu, C. Paz-Soldan, T. Markovic, H. Wang, Y. In, L. Piron, P. Piovesan, C. E. Myers, M. Maraschek, S. M. Wolfe, E. J. Strait, S. Munaretto, Empirical scaling of the $n = 2$ error field penetration threshold in tokamaks, *Nuclear Fusion* 60 (2020) 086010. URL: <http://dx.doi.org/10.1088/1741-4326/ab94f8>. doi:doi:10.1088/1741-4326/ab94f8.
- ³⁹D. A. Ryan, M. Dunne, A. Kirk, S. Saarelma, W. Suttrop, C. Ham, Y. Q. Liu, M. Willensdorfer, Numerical survey of predicted peeling response in edge localised mode mitigated and suppressed phases on ASDEX upgrade, *Plasma Physics and Controlled Fusion* 61 (2019) 095010. URL: <http://dx.doi.org/10.1088/1361-6587/ab32fa>. doi:doi:10.1088/1361-6587/ab32fa.
- ⁴⁰S. Munaretto, E. J. Strait, S. R. Haskey, N. C. Logan, C. Paz-Soldan, D. B. Weisberg, Modal analysis of the full poloidal structure of the plasma response to $n = 2$ magnetic perturbations, *Physics of Plasmas* 25 (2018) 072509. URL: <http://dx.doi.org/10.1063/1.5029381>. doi:doi:10.1063/1.5029381.
- ⁴¹Z. R. Wang, N. C. Logan, S. Munaretto, Y. Q. Liu, Y. W. Sun, S. Gu, J. K. Park, J. M. Hanson, Q. M. Hu, T. Strait, R. Nazikian, E. Kolemen, J. E. Menard, Identification of multiple eigenmode growth rates in DIII-D and EAST tokamak plasmas, *Nuclear Fusion* 59 (2019) 024001. URL: <http://dx.doi.org/10.1088/1741-4326/aaf671>. doi:doi:10.1088/1741-4326/aaf671.
- ⁴²Y. Liu, A. Kirk, L. Li, Y. In, R. Nazikian, Y. Sun, W. Suttrop, B. Lyons, D. Ryan, S. Wang, X. Yang, L. Zhou, Comparative investigation of ELM control based on toroidal modelling of plasma response to RMP fields, *Physics of Plasmas* 24 (2017) 056111. URL: <http://dx.doi.org/10.1063/1.4978884>. doi:doi:10.1063/1.4978884.
- ⁴³L. Zhou, Y. Liu, R. Wenninger, Y. Liu, S. Wang, X. Yang, Toroidal plasma response based ELM control coil design for EU DEMO, *Nuclear Fusion* 58 (2018) 076025. URL: <http://dx.doi.org/10.1088/1741-4326/aac602>. doi:doi:10.1088/1741-4326/aac602.

- ⁴⁴S. M. Yang, J. K. Park, N. C. Logan, C. Zhu, Q. Hu, Y. M. Jeon, Y. In, W. H. Ko, S. K. Kim, Y. H. Lee, Y. S. Na, Localizing resonant magnetic perturbations for edge localized mode control in KSTAR, Nuclear Fusion 60 (2020) 096023. URL: <http://dx.doi.org/10.1088/1741-4326/aba1cf>. doi:doi:10.1088/1741-4326/aba1cf.
- ⁴⁵N. C. Logan, C. Zhu, J. K. Park, S. M. Yang, Q. Hu, Physics basis for design of 3D coils in tokamaks, Nuclear Fusion 61 (2021) 076010. URL: <http://dx.doi.org/10.1088/1741-4326/abff05>. doi:doi:10.1088/1741-4326/abff05.